ISSN 1330-3651 (Print), ISSN 1848-6339 (Online)
Received: 24 March 2025; Accepted: 26 June 2025

https://doi.org/10.17559/TV-20250324002511
Original scientific paper

# Modelling and Trajectory Tracking Control of Multi Differential Wheel Heavy-Duty AGV Based on Koopman Operator

Xuehong ZHU*, Lizhen JIA, Shutong LIU, Zhuang GAO, Jingyang JI

**Abstract:** Automated guided vehicles (AGVs) are extensively applied in aerospace, ports, docks, rail transit, and other industries that require intelligent handling of heavy loads. Accurate modelling and trajectory tracking are crucial for performing the intelligent transfer of large objects and components using AGVs. To address the insufficient precision of current mathematical models and their inability to precisely perform trajectory tracking tasks due to the nonlinearity and strong coupling of multi differential wheel heavy-duty AGVs, a trajectory tracking control strategy based on the Koopman operator is proposed in this paper. First, based on the Koopman operator, an approximate high-dimensional linear dynamic explicit expression for the multi differential wheel heavy-duty AGV system is obtained using extended dynamic mode decomposition. Then, based on the obtained expression, a linear model predictive controller (MPC) is designed to achieve trajectory tracking control for heavy-duty AGVs. Finally, through simulation and experimental verification, it is demonstrated that the model information obtained from the data is effective and fits the dynamic model of the multi differential wheel heavy-duty AGV well. Comparisons reveal that its model accuracy is higher than that of the traditional Lagrange model; the root mean squared error (RMSE) and relative RMSE based on the Koopman model increase by an average of 24.86% and 3.24%, respectively. The designed linear model based on the Koopman operator can be combined with model predictive control. The controller can effectively perform trajectory tracking control, verifying its effectiveness. This work is the first experimental verification of the Koopman operator in heavy-duty AGV control, which will promote the engineering application of complex nonlinear systems.

**Keywords:** Chinese library classification (CLC) No; heavy-duty AGV; Koopman operator; model predictive control; trajectory tracking control;

## 1 INTRODUCTION

Multi-wheeled heavy-duty automated guided vehicles (AGVs) are wheeled mobile robots that are typical multi-input, multi-output, strongly coupled nonlinear time-variant systems [1]. It is especially important to study the trajectory tracking control strategies of heavy-duty AGVs to fulfill the intelligent handling capabilities of large-mass and overloaded deliveries, which are commonly required in several fields such as aerospace, shipbuilding, and railyards. Multi-wheel heavy-duty automated guided vehicles mainly face difficulties in modeling complex nonlinear systems in engineering applications, requiring high computational power and control accuracy to establish accurate models.

Traditional nonlinear systems are usually solved through nonlinear control methods, but due to the dimensionality and high nonlinearity of robot systems, it is difficult to achieve nonlinear real-time feedback control. In addition, dynamic parameters and unknown environments change in real time during robot motion, which requires real-time adjustment of nonlinear system model parameters, leading to increasing interest in real-time data-driven modeling and control methods. The main difficulty in this process is to explicitly represent the linearized model of the nonlinear system and integrate it with model-based control methods for application in engineering examples, which is also the main work of this paper.

The accuracy and effectiveness of AGV controls are current hotspots of academic and industrial research. For example, to address complex AGV path tracking problems while accounting for time constraints, a Lyapunov-based predictive control method was recently put forward [2] that successfully tracks a generated discrete set of reference path points by applying a quadratic planning method based on the double integrator technique, in which the reference path is segmented and constructed virtually. Separately, a 16-wheel heavy-duty AGV control model was adjusted for two-wheel requirements using the Ackermann steering principle [3] with a fuzzy trajectory control strategy based on the vehicle's accumulated driving experiences. A new dynamic coefficient convergence law was proposed to decrease the response time of a sliding mode control system for providing AGV trajectory tracking [4]. An adaptive learning-based model predictive control strategy was suggested for trajectory tracking of AGVs perturbed by input constraints, [5] and a real-time nonlinear model predictive control approach was introduced to perform online numerical computations using an extended/generalized minimum residual method [6]. A sliding mode control extended state observer design based on AGV error-tracking provided the ability to account for uncertain perturbations, such as sideslip, ground roughness, and friction [7].

Extensive research about the traditional trajectory tracking control methods relying on kinematic or dynamic models has been conducted. The control accuracy mainly depends on the precision of these models. However, the overly idealized design assumptions and nonlinear uncertainty greatly compound the difficulty in tracking, predicting, and controlling complex internal coupled AGV dynamic systems [8]. Therefore, the aforementioned studies are likely to cause inaccurate results, time-consuming and computationally expensive while also affecting performance.

Converting nonlinear modeling problems into linear form has become a very popular approach to addressing complex modeling tasks. Examples of linearization methods include segmental, [9] Taylor, [10] feedback, [11] and orthogonal function approximation types [12]. However, these methods all have limitations. With segmental methods, a large amount of information about the original nonlinear system is required, and the Taylor method works only at locally specific points; hence, only approximations of the original system can be provided. An accurate model is also needed for the feedback method, and the orthogonal function approximation method requires an oversized amount of data, which makes computations very

expensive. Therefore, an efficient linearization modeling method must be devised.

Koopman operator theory provides an accurate and simple linear modeling method for converting nonlinear dynamical systems into infinite-dimensional linear systems by utilizing the input–output data of the system itself [13]. This modeling process requires only simulation or experimental data and is completely different from traditional methods. The fundamental idea of the Koopman operator lies in lifting the state of the system into an infinite-dimensional space, within which the system can evolve linearly. This transformation, albeit at the expense of infinite dimensions, makes it possible to acquire a linear representation of the original system. Consequently, the original system is represented in a linear state space, enabling an accurate assessment of its behavior. However, at this juncture, the state transitions to a higher dimension, thereby achieving global linearization of nonlinear dynamical systems.

Distinct from black box models, such as neural networks and Gaussian processes, the Koopman operator has the capability to extract system dynamics information from operational data and establish explicit high-dimensional linear models. The integration of the Koopman operator with model-based linear control methods holds substantial theoretical value and practical significance. Derived from the Koopman operator, the high-dimensional linear model can reliably forecast the outputs of the system, and this model can be seamlessly integrated with linear control theory and model-based control methodologies. In theoretical terms, maximizing the expansion of the state to the subspace of the Koopman operator necessitates elevating the original state to an infinite-dimensional space. This implies that the Koopman operator is inherently infinite-dimensional, posing significant challenges and impracticalities for real-world applications. Therefore, it is significant in parctice to determine an accurate finite-dimensional approximation of the infinite-dimensional Koopman operator. Existing methods primarily encompass the DMD method and extended DMD method [15]. These two methods allow for the acquisition of the spectral characteristics of the Koopman operator and its infinite-dimensional approximation, to obtain an explicit linear expression. Both methods exhibit computational flexibility and ease of implementation, primarily relying on the least squares regression algorithm. This facilitates problem-specific expansion by researchers and offers a broad range of applications.

In current studies, more and more control design achievements appear, based on Koopman's theory. For example, to support shared driver-vehicle control, Guo etal. proposed an approach to capture the inherent dynamics characteristics of this system and generate an explicit control-oriented model using Koopman operator and the infinite dimensional space [16]. Separately, a model predictive control scheme based on an unbiased Koopman operator has been used to provide a practical way for modeling and directing soft manipulators [17]. The practicality of using a Koopman-based system identification method was utilized to develop three new MPCs that employ data-driven control schemes to evaluate trajectory-tracking performance in soft robots [18]. More recently, a deep learning-based Koopman representation method was utilized for model training, and a new MPC was proposed to control vehicle motion [19]. A decentralized data-driven control method based on an interconnected system was also developed, [20] and its effectiveness was verified through simulations involving two coupled Duffing oscillators, a bipedal motion model, and a four-tank system.

As indicated, the control strategy needed for the multi-wheeled heavy-duty AGV presented in this study should be Koopman-based, requiring no a priori system knowledge. A linear MPC controller that can transform the traditional nonlinear MPC into a linear version is also needed because the Koopman operator becomes linear after extended dynamic mode decomposition EDMD approximation. This process avoids nonconvex optimizations and enables compliance with real-time requirements.

The theoretical contribution of this paper lies in the pioneering application of the Koopman operator to the modeling and control of multi-wheel differential heavy-duty automatic guided vehicles (AGVs), particularly in scenarios where model parameters and dynamic models are entirely unknown. We propose an efficient high-dimensional linear dynamic model, upon which a linear model predictive controller (MPC) is subsequently developed for precise trajectory tracking. This work showcases that our method can be seamlessly integrated with linear control theory and model-based control techniques, thereby advancing this research area.

The organization of the remaining part of this paper is as follows. In Section 2, the Koopman operator modeling process is presented, and its representation method for the controlled heavy-duty AGV system is given. In Section 3, the MPC control strategy relying on Koopman high - dimensional linear model is elaborated. Section 4 verifies the feasibility, practicality of the model and the effectiveness of the Koopman-based trajectory tracking control strategy. Finally, Section 5 delivers the conclusion and offers insights for future research directions.

## 2 KOOPMAN OPERATOR MODELING

To predict the next state or multiple states for a multi-wheeled heavy-duty AGV nonlinear system, this study explores the application of Koopman operator due to its ability to address the prblems in an infinite-dimensional linear system. More details on Koopman operator theory can be found in the literature. The modeling evolution diagram for multi-wheeled heavy-duty AGVs using the Koopman operator is shown in Fig. 1.

Considering a controlled dynamic multi-wheeled heavy-duty AGV system,

$$x(k+1) = f(x(k), \tau(k)) \tag{1}$$

where $x(k)$ denotes the state vector, and $\tau(k)$ representes the control input torque vector, both at time *k*.

We define a set of basis (lifted) functions in the Koopman high-dimensional subspace as $\Psi(x) = \begin{bmatrix} \varphi_1(x) & \varphi_2(x) & \cdots & \varphi_n(x) \end{bmatrix}^T$, and the observation

function of the linear combination of these basis functions is

$$g(x)=\sum_{k=1}^{n}\alpha_k\varphi_k(x)=\Psi(x)\alpha \tag{2}$$

where $\alpha$ is the coefficient matrix.

It is further given that

$$(\kappa g)(x)=g\circ f(x)=\kappa\Psi(x)\alpha+r(x), \tag{3}$$

where $r(x)$ is the residual term.

Regarding the control system defined by Eq. (1), an approximation of the Koopman operator based on the extended dynamic modal decomposition method [15] supplies the necessary operator approximation operator:

$$\min_{\kappa}\frac{1}{2}\sum_{k=0}^{N-1}\left\|\Psi(\chi(k+1))-\kappa\Psi(\chi(k))\right\|^2, \tag{4}$$

where $\chi(k)=[x(k),\tau(k)]^T$,

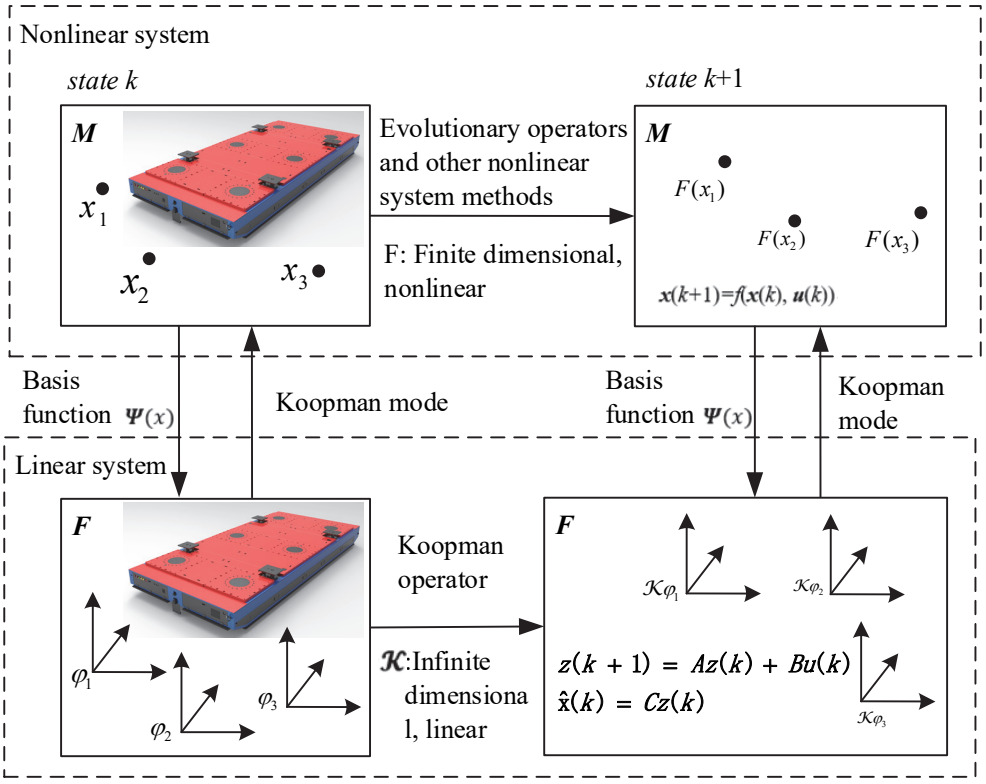


**Figure 1** Model evolution diagram of heavy-duty AGVs based on the Koopman operator

The form of the high-dimensional linear model obtained based on the Koopman operator is as follows:

$$\begin{aligned}h(k+1)&=Ah(k)+B\tau(k)\\ z(k)&=Ch(k)\end{aligned}, \tag{5}$$

where $h(k)\in\mathbb{R}^N$ denotes the state after lifting $N$ dimensions, and $z(k)$ stands for the estimated output of the original system state, $x(k)$, as determined using Koopman operator theory. $A\in\mathbb{R}^{N\times N}$, $B\in\mathbb{R}^{N\times M}$, and $C\in\mathbb{R}^{M\times N}$, are constant matrices.

The system state dataset is modeled as follows:

$$\begin{aligned}X&=[x(1),\ldots,x(P)]\\ Y&=[x(2),\ldots,x(P+1)]\\ T&=[\tau(1),\ldots,\tau(P)]\end{aligned}. \tag{6}$$

We collect the lifted state dataset as

$$\begin{aligned}X_{\text{lift}}&=[\Psi(x(1)),\ldots,\Psi(x(P))]\\ Y_{\text{lift}}&=[\Psi(x(2)),\ldots,\Psi(x(P+1))]\end{aligned}. \tag{7}$$

The $A$, $B$, and $C$ matrices are solved with the following optimization problem:

$$\min_{A,B}\left\|Y_{\text{lift}}-AX_{\text{lift}}-BT\right\|, \tag{8}$$

$$\min_{C}\left\|X_{\text{lift}}-CX_{\text{lift}}\right\|. \tag{9}$$

The solution is then given by

$$\begin{aligned}[A,B]&=Y_{\text{lift}}\left[X_{\text{lift}},T\right]^{\dagger}\\ C&=XX_{\text{lift}}^{\dagger}\end{aligned}, \tag{10}$$

where † denotes the Moore-Penrose pseudo-inverse.

Finally, the Koopman high-dimensional linear pre-model derived from Eq. (5) is used to substitute the original heavy-duty AGV dynamic system of Eq. (1).

## 3 CONTROL STRATEGY DESIGN

A valid model predictive control accounts for various constraints while predicting future output scenarios over a fixed period. Optimized control is achieved when applying the optimized input at one time step and performing iterative optimization thereafter [21]. Approaches to dealing with linear and nonlinear systems in model predictive control scenarios are similar, but nonlinear problems are too complex and time-consuming to solve in real time. Koopman linear models can transform nonlinear problems into linear ones to avoid nonconvex optimization problems.

Therefore, MPCs can be designed for trajectory tracking control for multi-wheeled heavy-duty AGVs. With respect to Eq. (5), which incorporates the Koopman operator, the prediction equation for any future state is as follows:

$$\begin{aligned} h(k+1\,|\,k) &= Ah(k)+B\tau(k)\\ h(k+2\,|\,k) &= Ah(k+1\,|\,k)+B\tau(k+1\,|\,k)\\ &\vdots\\ h(k+N_c\,|\,k) &= Ah(k+N_c-1\,|\,k)+B\tau(k+N_c-1\,|\,k)\\ &\vdots\\ h\left(k+N_p\,|\,k\right) &= Ah\left(k+N_p-1\,|\,k\right)+B\tau\left(k+N_c-1\,|\,k\right) \end{aligned} \tag{11}$$

The predicted output equation is compact and expressed as follows:

$$\begin{aligned} Z(k) &= Fz(k)+\Phi T(k)\\ Z(k) &= \left[z(k+1|k)^T,\cdots,z\left(k+N_p\,|k\right)^T\right]^T\\ T(k) &= \left[\tau(k)^T,\ldots,\tau\left(k+N_c-1|k\right)^T\right]^T\\ F &= \left[CA,CA^2,\ldots,CA^{N_p}\right]^T \end{aligned} \tag{12}$$

$$\Phi=\begin{bmatrix} CB & 0 & \cdots & 0\\ CAB & CB & \ldots & 0\\ \vdots & \vdots & \ddots & \vdots\\ CA^{N_p-1}B & CA^{N_p-2}B & \ldots & CA^{N_p-N_c}B \end{bmatrix}$$

The reference trajectory in the predicted time domain is given by

$$Z_r(k)=\left[z_r(k+1)^T,\ldots,z_r\left(k+N_p\right)^T\right]^T. \tag{13}$$

The model predictive control aims at minimizing the following performance indicator function:

$$\begin{aligned} J=&\left(Z(k)-Z_r(k)\right)^T Q\left(Z(k)-Z_r(k)\right)\\ &+T(k)^T RT(k) \end{aligned}, \tag{14}$$

where $Q$ and $R$ are diagonal matrices.

The above equation is equivalent to

$$\begin{aligned} &\min_T J \Rightarrow \min_T \hat{J}\\ &\text{s.t. } h(i+1)=Ah(k)+B\tau(k)\\ &\quad h=\Psi(x) \end{aligned}, \tag{15}$$

where

$$\begin{aligned} \hat{J} &= 2T\left(k\right)^T H+T\left(k\right)^T ET\left(k\right)\\ H &= \Phi^T Q\left(Fh\left(k\right)-Z_r\left(k\right)\right)\\ E &= \Phi^T Q\Phi+R\\ Q &= \mathrm{diag}\left(\overbrace{Q_a,Q_a,\ldots,Q_a}^{N_p},QN_p\right)\\ R &= \mathrm{diag}\left(\overbrace{R_c,R_c,\ldots,R_c}^{N_c}\right) \end{aligned} \tag{16}$$

These equations can be quickly solved as a standard linear quadratic programming problem. By solving Eq. (19), the optimal control sequence in the predicted range, $N_p$, will be achieved. The first element in $T(k)$ is the output torque at time $k$. At this point, the optimal control input $T$, is obtained. The control structure block diagram is shown in Fig. 2.

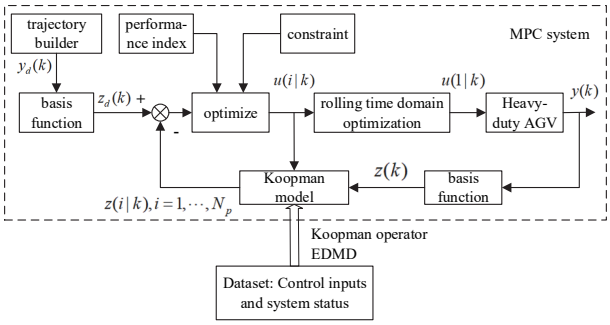


**Figure 2** Multi-wheeled heavy-duty AGV control structure block diagram

## 4 EXPERIMENT AND ANALYSIS

### 4.1 Establishment of Experimental Environment

The multi-wheeled heavy-duty AGV platform used in this study had six differential drive units of two drive wheels each, resulting in 12 wheels. Each drive wheel contained a single 1.5 kW direct-current motor with a reduction rate of 100. The power supply voltage was 48 V. The core controller of the heavy-duty AGV was a UNO-3285G with an i7-6822EQ processor with 8-GB RAM and two built-in controller area network (CAN) cards. One CAN card was connected to the drive and motor-end encoder, and the other was connected to the rotary encoder for all six differential drive units. The construction and comprehensive analysis of high-dimensional linear dynamic models were executed utilizing MATLAB software, renowned for its precision and robustness in numerical computations. For the purpose of trajectory tracking simulation, the Simulink module within MATLAB was employed, offering a dynamic and intuitive environment for modeling and simulating complex systems. Furthermore, the control system for the

experimental prototype was developed leveraging the ROS (Robot Operating System) platform, which facilitates the creation of robust and scalable robotic applications. The algorithm was meticulously coded using VSCode, an advanced code editor, and Python, a versatile programming language suited for scientific computing. Lastly, the visualization component was developed using the Rviz module within ROS, providing a detailed and interactive representation of the system's behavior. Rviz is a 3D visualization tool within the Robot Operating System (ROS) designed for displaying and debugging sensor data, status information, and motion planning of robots. It enables the graphical representation of various relevant data, encompassing robot models, sensor data, environmental maps, and more. This article also used MATLAB software for simulation experiments. This integrated approach ensures the accuracy, efficiency, and scalability of the proposed methods and systems.The real multi-wheeled heavy-duty AGV is pictured in Figure 3. Tab. 1 lists the technical parameters of the heavy-duty AGV.

**Figure 3** Real heavy-duty AGV

**Table 1** Technical parameters of the heavy-duty AGV

| Symbol | System parameter | Value (units) |
|---|---|---|
| $m$ | Heavy load AGV vehicle weight | 10 000 kg |
| $h$ | Distance between rotation centers of adjacent differential drive units in the length direction of the heavy-duty AGV | 2 m |
| $s$ | Half the distance between the rotation centers of two sets of differential drive units in the width direction of the heavy-duty AGV | 0.8 m |
| $d$ | Half the distance between the two wheel centers of the differential drive unit | 0.29 m |
| $r$ | Heavy load AGV wheel radius | 0.167 m |
| $J_0$ | Rotational inertia of the heavy-duty AGV | 7941.7 kg·m$^2$ |
| $J_1$ | Moment of inertia of the heavy-duty AGV wheels | 0.558 kg·m$^2$ |
| $T$ | Rated torque of the motor | 5 N·m |
| $n$ | Reduction ratio of the motor reducer | 100 |
| $p$ | Motor power | 1.5 kW |

## 4.2 Determination of Basis Functions and Dimensionality Enhancement

Choosing different types of basis functions will have an impact on the approximation performance of Koopman high-dimensional subspaces. Higher order basis functions may lead to overfitting, while lower order basis functions may lose important features of the system. Therefore, it is necessary to make reasonable trade-offs when selecting basis functions and adjust them based on the properties of the actual system to achieve better dynamic approximation results. For the selection of basis functions, there are currently two commonly used types: Hermitian polynomials and radial basis functions. Hermitian polynomials are generally used for data that follow a normal distribution, while radial basis functions are generally used for problems defined on irregular domains. This article selects the thin plate spline radial basis function with the center located at $x_0$ as the basis function, that is, $\psi(x) = \| x - x_0 \|^2 \log(\| x - x_0 \|)$, $x_0$ is a constant vector of elements uniformly distributed within a given interval.

To determine the optimal dimensionality for dimension expansion, relevant experiments were designed, and simulation data were used for system testing. The test dimension range is 0-20 dimensions (the corresponding actual Koopman model dimensionality ranges from 30 to 50). Because when the dimensionality exceeds 20, the Root Mean Squared Error (*RMSE*) and Relative Root Mean Squared Error (*RRMSE*) will exceed 100% and the accuracy of the system model will greatly decrease. During the experiment, 10 repeated tests were conducted to evaluate the *RMSE* and *RRMSE* between the Koopman models with varying dimensionalities and the true model. The average values over 10 tests show that RMSE and RRMSE increase as the test dimensionality rises. When the test dimensionality is 1 (Koopman model dimensionality is 31), the *RMSE* and *RRMSE* reach their lowest values. Therefore, this paper sets the dimensionality to 1. The *RMSE* and *RRMSE* of the heavy-duty AGV under different expansion dimensionalities are shown in Fig. 4.

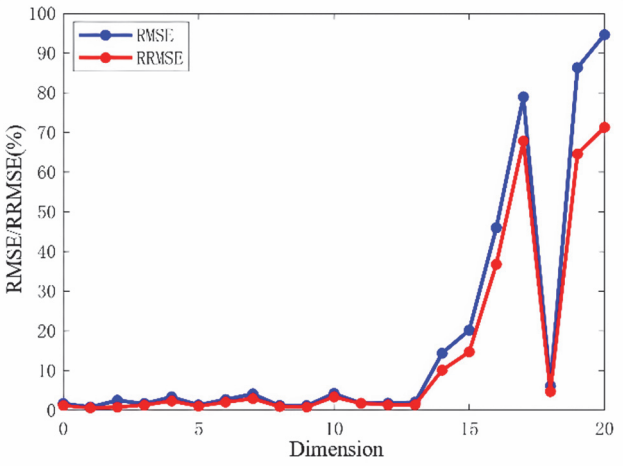


**Figure 4** RMSE and RRMSE of heavy-duty AGV in different dimensions

## 4.3 Model Accuracy Verification

The flowchart of the heavy-duty AGV experiment is shown in Fig. 5.

To further measure the effectiveness of the two approaches, the root mean square error (*RMSE*) and relative *RMSE* (*RRMSE*) were used to compare the Koopman and Lagrange models.

$$RMSE = \sqrt{\frac{\sum_{i=1}^{N} \| x_{ki} - x_{ti} \|_2^2}{N}} \tag{17}$$

$$RRMSE = \frac{\sqrt{\sum_{i=1}^{N} \left\| x_{ki} - x_{ti} \right\|_2^2}}{\sqrt{\sum_{i=1}^{N} \left\| x_{ti} \right\|_2^2}} \tag{18}$$

Here, $x_{ki}$ presents the predicted data based on Koopman, $x_{ti}$ presents the real data of the overloaded AGV, $N$ is the total number of experimental data points collected, and $\left\| x_{ki} - x_{ti} \right\|_2^2$ presents $xy\ \theta$, the state norm.

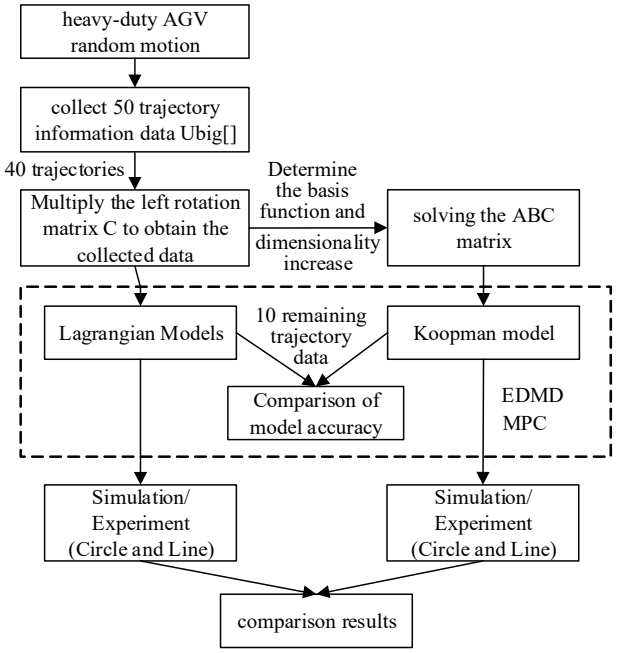


**Figure 5** Experimental flowchart of the heavy-duty AGV

In the context of acquiring the experimental dataset, it is postulated that the heavy-duty AGV operates in a normal fashion, devoid of any slip or lateral slip phenomena. To ascertain the optimal input torque, the following strategic constraints are enforced:

Strategic Constraints:

1) Torque Synchronization: The two motors within each differential drive unit must generate torque in unison. Any deviation in their direction would induce in-place rotation of the differential drive unit, ultimately leading to slip in the heavy-duty AGV.
2) Instantaneous Center Calculation: The instantaneous center can be deduced from the torque output of one differential drive unit set, the steering angle of another set, and the torque exerted by one motor from the remaining five sets of differential drive units. Leveraging the sine theorem, the torque output and steering angle for the remaining five sets of differential drive units can be accurately computed.

The randomly changing input torque experienced during the experiment damaged the motors because it conflicted with the kinematic constraints of the AGV. Therefore, the experimental data were obtained by manually controlling the AGV along a random path. Encoder feedback was taken from the end of each motor, and each differential drive unit was equipped with a rotary encoder in the middle position to read the speed and torque in real time. A total of 50 motion trajectory data items were collected during the experiment at a sampling time of 25 s per trajectory. This resulted in a sampling period of $\Delta T$ = 0.05 s and 25,000 data items. A total of 40 trajectory data items were selected, and when fitting the Koopman high-dimensional linear model, the remaining 10 items were used as test data to evaluate the accuracy of the solution.

The comparison of model accuracy involved real, Koopman, and Lagrangian trajectories. The ground-truth trajectory was preserved from the real-time data, which were displayed in the Rviz module of the robot operating system, as shown in Fig. 6. The results of its motor output torque are displayed in Fig. 7. The Koopman model trajectory used the high-dimensional linear model, and the Lagrangian trajectory was calculated using Lagrangian dynamics. Fig. 8 shows a comparison of trajectory effects under different AGV models. Notably, the Koopman model gave better results than the traditional Lagrangian type and effectively fitted the real trajectory. It is important to ensure that both models have analogous control inputs in the same initial states when the models are compared, owing to input constraint issues that limit the stochastic data's ability to fit the real engineering conditions.

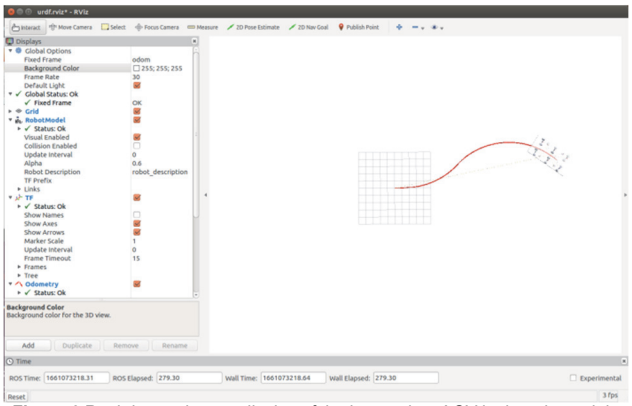

**Figure 6** Real-time trajectory display of the heavy-duty AGV in the rviz module

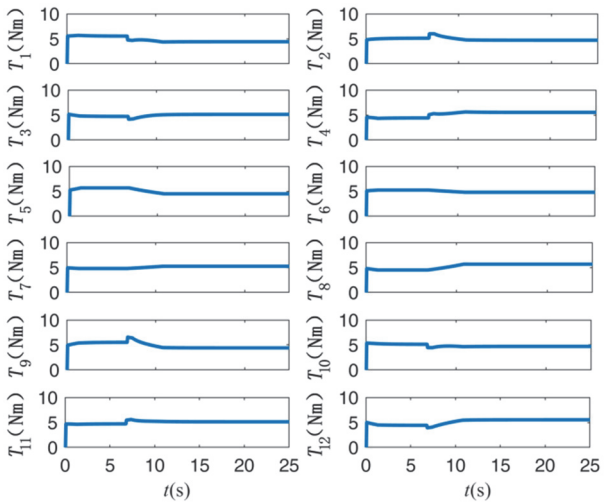


**Figure 7** Output torque diagrams of motors in heavy duty AGV

Using the remaining 10 sets of random motion trajectory data for model accuracy testing, the testing indicators are RMSE and RRMSE. As seen in Tab. 2, the RMSE and RRMSE of the Koopman-based model both show superior (smaller) results over the Lagrange model by 24.86% and 3.24%, respectively. This implies that the

Koopman model better fits the scenario, is more similar to the real process, and can be used for model-based control design.

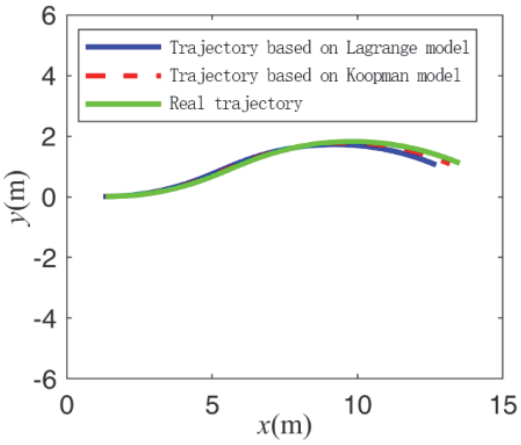


**Figure 8** Comparison of trajectories under different models

**Table 2** *RMSE* and *RRMSE* results

| Group no. | RMSE / % | | RRMSE / % | |
|---|---|---|---|---|
| | Lagrange | Koopman | Lagrange | Koopman |
| 1 | 49.77 | 20.70 | 5.98 | 2.21 |
| 2 | 46.72 | 18.67 | 5.26 | 2.03 |
| 3 | 35.97 | 14.75 | 4.16 | 1.22 |
| 4 | 41.17 | 17.65 | 4.95 | 1.69 |
| 5 | 41.53 | 17.82 | 4.97 | 1.72 |
| 6 | 44.85 | 18.69 | 5.17 | 1.95 |
| 7 | 40.64 | 17.55 | 4.72 | 1.58 |
| 8 | 42.13 | 18.30 | 5.02 | 1.87 |
| 9 | 41.79 | 17.96 | 4.99 | 1.76 |
| 10 | 44.66 | 18.55 | 5.19 | 1.92 |
| Mean value | 42.92 | 18.06 | 5.04 | 1.80 |

### 4.4 Trajectory-Tracking Experiment

The parameters used in the MPC were set as follows:

$$\begin{aligned} Q_a &= \mathrm{diag}(6,8,8,8,8,8,8,8,8,8,8,8,8,8,8) \\ Q_N &= 100 * \mathrm{diag}(2,3,3,3,3,3,3,3,3,3,3,3,3,3,3) \\ R_c &= 1\times10^{-5} * \mathrm{diag}(5,5,4,7,7,7,7,7,7,7,7,7,7) \end{aligned} \quad (19)$$

(1) Linear trajectory experiment

The experimental results of the multi-wheeled heavy-duty AGV where the desired trajectory is a straight line are shown in Figs. 9 to 12.

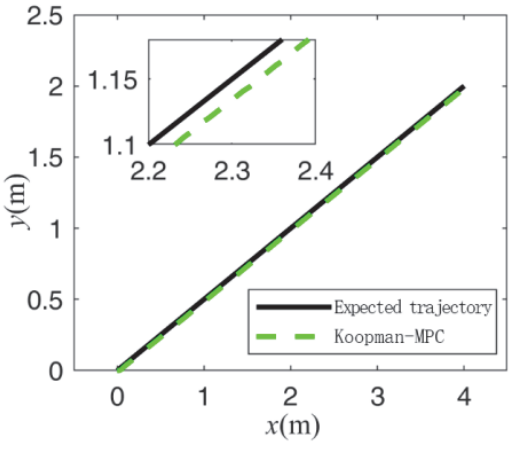


**Figure 9** Straight trajectory experiment

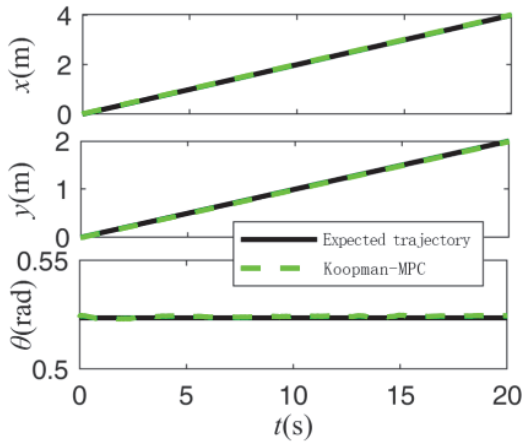


**Figure 10** Pose tracking experiment results of heavy duty AGV linear trajectory

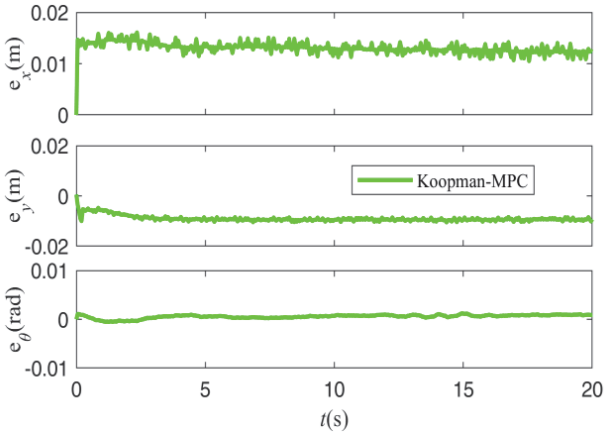


**Figure 11** Straight trajectory tracking error

As seen in Figs. 8 and 9, the Koopman-based MPC controller achieved tracking control of the multi-wheeled heavy-duty AGV linear trajectory with an error of within 2 cm when there was no initial error. It can be seen in Fig. 10 that there is still a certain degree of error in this controller at approximately 15 mm in the $x$-direction, 10 mm in the $y$-direction, and 0.001 rad in the $\theta$-direction. Fig.11 shows the output torque of each motor of the multi-wheeled heavy-duty AGV during the experiment, revealing that this MPC outputs the torque relatively smoothly during the experiment.

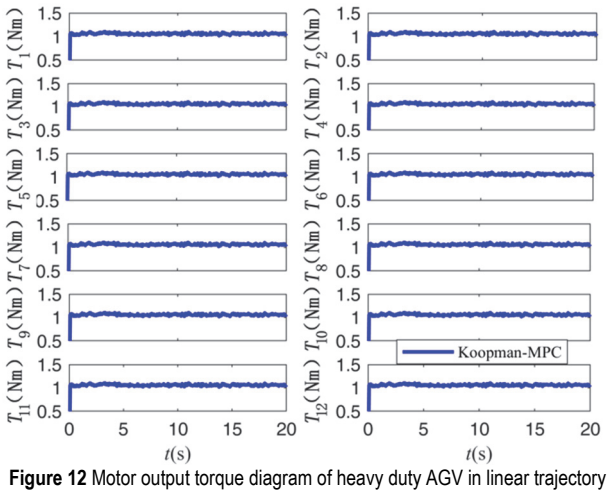


**Figure 12** Motor output torque diagram of heavy duty AGV in linear trajectory

(2) Circular trajectory experiment

The experimental results of a circular trajectory are shown in Figs. 13 to 16. As seen in Figs. 12 and 13, the Koopman-based MPC achieved tracking control of the AGV trajectory very well when there was no initial error.

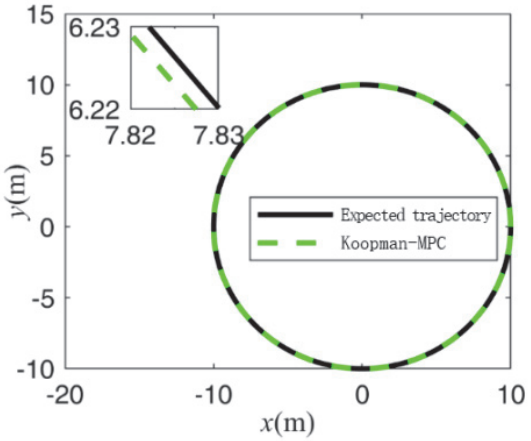


**Figure 13** Circular trajectory experiment

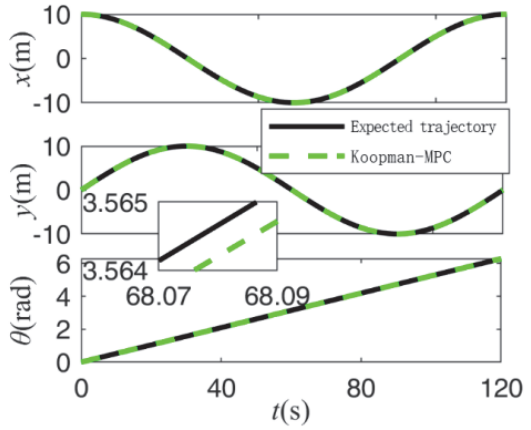


**Figure 14** Pose tracking experiment results of heavy duty AGV circular trajectory

Fig. 14 shows that there was still a certain degree of error in this controller at approximately 17 mm in the $x$-direction, 12 mm in the $y$-direction, and 0.002 rad in the $\theta$-direction. Fig. 15 shows the motor output torque diagram of the AGV from the circular trajectory experiment. Clearly, the MPC controller has some slight errors in the output torque during the experiment, and the output torque is greatly affected by environmental disturbances.

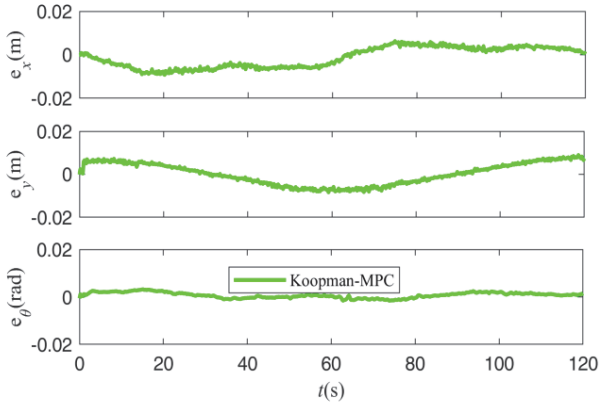


**Figure 15** Circular trajectory tracking error

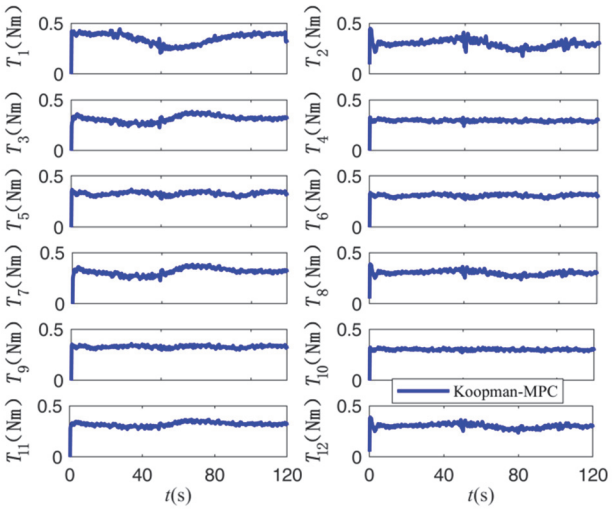


**Figure16** Motor output torque diagram of heavy duty AGV in circular trajectory

Overall, the Koopman-based control strategy, lacking a priori knowledge, performs well in trajectory tracking tasks for both linear and circular reference trajectories, resulting in a satisfactory performance overall. The experiments show that the proposed strategy exhibits good tracking effects on the multi-wheeled heavy-duty AGV, and the method provides a direct and effective solution for realizing the modeling and control of multi-wheeled robots in complex situations with incomplete constraints.

## 5 CONCLUSION AND OUTLOOK

In this paper, a model based on the Koopman operator and a trajectory tracking control strategy were designed for a multi-wheeled heavy-duty AGV trajectory tracking control task, and real trajectory tracking control experiments were performed. First, a Koopman linearized high-dimensional model was obtained directly from ground-truth data using an extended dynamic modal decomposition method to approximate the Koopman operator, and the MPC framework was used complementarily. The results showed that the high-dimensional linear model achieved by the extended dynamic modal decomposition approximation method was relatively accurate and effective; hence, it can be used for the improved model-based control design. Subsequent results showed that the designed controller performed relatively well and consumed less time, which ensured a certain degree of timeliness. It not only tracked the reference trajectory quickly and stably but also maintained the precision of the actual trajectory within 0.02 m.

This was the first time that this type of control scheme was implemented for the real-world operation of a multi-wheeled heavy-duty AGV. In future endeavors, we aim to integrate the sliding mode control method, nonlinear model predictive control method, and linear quadratic regulator, among others, for comprehensive verification. This will involve assigning distinct weights to penalize terminal states, taking into account factors such as data sparsity and information interference. If they can be addressed, online data modeling can be achieved, improving the accuracy of the built model and reducing control time delays. Additionally, we will employ effective basis functions for

validation purposes, with the ultimate goal of enhancing trajectory tracking performance even further.

**Acknowledgements**

The Science & Technology Development Fund of Tianjin Education Commission for Higher Education (ID: 2023KJ243).

## 6 REFERENCES

[1] Cui, M., Liu, W., Liu, H., Jiang, H., & Wang, Z. (2016). Extended state observer-based adaptive sliding mode control of differential-driving mobile robot with uncertainties. *Nonlinear Dynamics*, *83*(1-2), 667-683. https://doi.org/10.1007/s11071-015-2355-z

[2] Zhang, S., Xia, Q., Cheng, S., Chen, M., & Xiao, G. (2022). Research on Lyapunov-based predictive path following control of AGV based on time constraint. *International Journal of Control, Automation, and Systems*, *20*(12), 4005-4014. https://doi.org/10.1007/s12555-021-0492-3

[3] Zhou, X., Jin, L., & Liu, Y. (2021). Modeling and simulation research of heavy-duty AGV tracking control system based on magnetic navigation. *Journal of Physics Conference Series*, *1746*, 012021. https://doi.org/10.1088/1742-6596/1746/1/012021

[4] Han, Y., Cheng, Y., & Xu, G. (2019). Trajectory tracking control of AGV based on sliding mode control with the improved reaching law. *IEEE Access*, *7*, 20748-20755. https://doi.org/10.1109/access.2019.2897985

[5] Zhang, K., Sun, Q., & Shi, Y. (2021). Trajectory tracking control of autonomous ground vehicles using adaptive learning MPC. *IEEE Transactions on Neural Networks and Learning Systems*, *32*(12), 5554-5564. https://doi.org/10.1109/tnnls.2020.3048305

[6] Liu, X., Wang, G., & Chen, K. (2021). Nonlinear model predictive tracking control with c/gmres method for heavy-duty agvs. *IEEE Transactions on Vehicular Technology*, *70*(12), 12567-12580. https://doi.org/10.1109/tvt.2021.3123176

[7] Pu, C., Ren, J., & Fang, G. (2021). Sliding mode control of AGV based on extended state observer. *Modern industrial IoT, big data, and supply chain: Proceedings of the IIoTBDSC.218*, 103-110. https://doi.org/10.1007/978-981-33-6141-6_11

[8] Villagra, J. & Herrero-Pérez, D. (2012). A comparison of control techniques for robust docking maneuvers of an AGV. *IEEE Transactions on Control Systems Technology*, *20*(4), 1116-1123. https://doi.org/10.1109/tcst.2011.2159794

[9] Pasolli, P. & Ruderman, M. (2018). Linearized piecewise affine in control and states hydraulic system: Modeling and identification. *44th annual conference of the IEEE Industrial Electronics Society*, 4537-4544. https://doi.org/10.1109/iecon.2018.8591572

[10] Wen, T. & Fang, J. C. (2012). A feedback linearization control for the nonlinear 5-DOF flywheel suspended by the permanent magnet biased hybrid magnetic bearings. *Acta Astronaut*, *79*, 131-139. https://doi.org/10.1016/j.actaastro.2012.04.017

[11] Umlauft, J. & Hirche, S. (2020). Feedback linearization based on Gaussian processes with event-triggered online learning. *IEEE Trans Automat Control*, *65*(10), 4154-4169. https://doi.org/10.1109/tac.2019.2958840

[12] Keyvan, A. B., Hosein, G., & Amir, Y. (2019). Orthogonal function-based equivalent linearization for sliding mode control of nonlinear systems. *Structural Control and Health Monitoring*, *26*(8), e2372.1-e2372.14. https://doi.org/10.1002/stc.2372

[13] Korda, M. & Mezić, I. (2018). Linear predictors for nonlinear dynamical systems: Koopman operator meets model predictive control. *Automatica*, *93*, 149-160. https://doi.org/10.1016/j.automatica.2018.03.046

[14] Hemati, M. S., Williams, M. O., & Rowley, C. W. (2014). Dynamic mode decomposition for large and streaming datasets. *Physics of Fluids*, *26*(11), 111701. https://doi.org/10.1063/1.4901016

[15] Williams, M. O., Kevrekidis, I. G., & Rowley, C. W. (2015). A data-driven approximation of the Koopman operator: Extending dynamic mode decomposition. *Journal of Nonlinear Science*, *25*(6), 1307-1346. https://doi.org/10.1007/s00332-015-9258-5

[16] Guo, W., Zhao, S., Cao, H., Yi, B., & Song, X. (2023). Koopman operator-based driver-vehicle dynamic model for shared control systems. *Applied Mathematical Modelling*, *114*, 423-446. https://doi.org/10.1016/j.apm.2022.10.014

[17] Chen, J., Dang, Y., & Han, J. (2022). Offset-free model predictive control of a soft manipulator using the Koopman operator. *Mechatronics*, *86*, 102871. https://doi.org/10.1016/j.mechatronics.2022.102871

[18] Bruder, D., Fu, X., Gillespie, R. B., Remy, C. D., & Vasudevan, R. (2021). Data-driven control of soft robots using Koopman operator theory. *IEEE Transactions on Robotics,37*(3), 948-961. https://doi.org/10.1109/tro.2020.3038693

[19] Wang, R., Han, Y., & Vaidya, U. (2021). Deep Koopman data-driven control framework for Autonomous racing. *Proceedings of the international conference on robotics automation: Workshop opportunities challenges in autonomous racing*, 1-6. https://doi.org/10.13140/RG.2.2.21512.75526

[20] Tellez-Castro, D., Garcia-Tenorio, C., Mojica-Nava, E., Sofrony, J., & Vande Wouwer, A. (2022).Data-driven predictive control of interconnected systems using the Koopman operator. *Actuators*, *11*(6), 151. https://doi.org/10.3390/act11060151

[21] Paulson, J. A., Mesbah, A., Streif, S., Findeisen, R., & Braatz, R. D. (2014). Fast stochastic model predictive control of high-dimensional systems. *53rd IEEE Conference on Decision and Control*, 2802-2809. https://doi.org/10.1109/cdc.2014.7039819

**Contact information:**

**Xuehong ZHU**, Lecturer
(Corresponding author)
School of Mechanical Engineering,
Tianjin Sino-German University of Applied Sciences, 300350, China
E-mail: jishezxh@163.com

**Lizhen JIA**, Lecturer
School of Transportation Science and Engineering,
Civil Aviation University of China, 300300
E-mail: jializhen_1314@163.com

**Shutong LIU**, Student
School of Mechanical Engineering,
Tianjin Sino-German University of Applied Sciences, 300350, China
E-mail: 1511881917@qq.com

**Zhuang GAO**, Student
Intelligent Manufacturing College,
Tianjin Sino-German University of Applied Sciences, 300350, China
E-mail: 2723735835@qq.com

**Jingyang JI**, Student
School of Automation and Electrical Engineering,
Tianjin University of Technology and Education, 300222, China
E-mail: 1679629536@qq.com